

**Errors in dynamical fields inferred from oceanographic cruise data.
Part II: the impact of the lack of synopticity.**

Damià Gomis⁽¹⁾, Ananda Pascual^(1,2) and Mike A. Pedder⁽³⁾

⁽¹⁾ Grup d'Oceanografia Interdisciplinar, IMEDEA (UIB-CSIC)
Campus UIB. 07071 Palma de Mallorca (Spain)
damia.gomis@uib.es

⁽²⁾ Space Oceanography Division, Collecte Localisation Satellite
8-10 rue Hermes, Parc Technologique du Canal. 31526 Ramonville Saint-Agne (France)
apascual@cls.fr

⁽³⁾ Department of Meteorology, University of Reading
2, Earley Gate, Reading RG6 6BB (UK)
m.a.pedder@reading.ac.uk

November 30, 2004

Corresponding author address: Damià Gomis, Dep. de Física,
Universitat de les Illes Balears.
07071 Palma de Mallorca, Spain
Tel.: +34 971 173236
Fax: +34 971 173426

ABSTRACT

Diagnostic studies of ocean dynamics based on the analysis of oceanographic cruise data are usually quite sensitive to observation errors, to the station distribution and to the synopticity of the sampling. The first two sources have been evaluated in Part I of this work. Here we evaluate synopticity errors for different sampling strategies applied to simulated unstable baroclinic waves. As suggested in previous studies, downstream and upstream cross-front samplings produce larger errors than along-front samplings. In our particular case study, the along-front sampling results in fractional errors (rms error divided by the standard deviation of the field) of about 15% for dynamic height and more than 50% for relative vorticity and vertical velocity. These values are significantly higher than those obtained in Part I for typical observation errors and sampling limitations (about 6% for dynamic height and between 15 and 30% for geostrophic vorticity and vertical velocity).

We also propose and test two methods aimed at reducing the impact of the lack of synopticity. The first one corrects the observations using the quasi-geostrophic tendency equation. The second method combines the relocation of stations (based on a system velocity) and the correction of observations (through the estimation of a growth rate). For the fields simulated in this work, the second method gives better results than the first, being able to eliminate practically all synopticity errors in the case of the along-front sampling. In practice, the error reduction is likely to be less effective, since actual fields cannot be expected to have a system velocity as homogeneous as for the single-mode waves simulated in this work.

Key words: synopticity errors; sampling; oceanographic surveys; vertical motion; dynamical oceanography.

1. INTRODUCTION

Within the last 20 years, diagnostic studies of ocean dynamics have evolved along with observational and theoretical developments. Presently, studies are undertaken even at the mesoscale and are increasingly based on the analysis of dynamically relevant variables such as potential vorticity or the vertical velocity component. These dynamical fields are often inferred directly from spatial distributions of observed variables assuming some kind of balance condition (e.g., the quasi-geostrophic theory, hereafter QG; see Part I of this work for a more detailed introduction). This involves the computation of spatial derivatives of observed fields, which have often been recognized as sensitive to observation errors, to the distribution of stations and to the lack of synopticity of the sampling.

The first two error sources have been examined in Part I of this work, focusing on the retrieval of mesoscale structures represented by a Gaussian correlation model with a characteristic scale of 15 km (which roughly corresponds to an anomaly field characterized by structures of about 45 km diameter). Results were that for a high density (SeaSoar) survey, rms errors relative to the standard deviation of the field (hereafter “fractional errors”) are of the order of 2% for dynamic height and about 5% for geostrophic vorticity and vertical velocity. These values refer to the inner domain, since errors increase up to 20% near the boundaries. For less dense (e.g. 10 km spaced CTD) samplings, fractional errors are up to 6% for dynamic height and 15% for geostrophic vorticity and vertical velocity (30% near the boundaries). The applied formulation assumes that actual fields obey the correlation model used for the interpolation of observations, which is not exactly the case in practice. Consequently, the results of that analysis should be regarded as establishing realistic lower bounds on the accuracy of parameters diagnosed from synoptic survey data.

The evaluation of the third error source, the lack of synopticity, has traditionally received less attention. This is perhaps because its impact is more case-to-case dependent and therefore it cannot be formulated in such a general way as for the other two error sources. However, the concerns about this problem increased significantly when diagnostic studies started to focus at the mesoscale. The reason is that even using fast sampling techniques such as towed CTD probes (e.g., Pollard, 1986; Allen et al, 1992) and ship-mounted Acoustic Doppler Current Profilers (e.g., Joyce, 1989; Gomis et al, 2001), the

time scales associated with mesoscale features are usually not much longer than the sampling period. As a consequence, the retrieval of observed fields can be seriously handicapped by the presence of significant mesoscale variability, as already reported by Matthews (1997).

A pioneering attempt to examine the impact of the lack of synopticity on the computation of derived magnitudes such as the vertical velocity was undertaken by Allen et al. (2001). More recently, Rixen et al. (2003) checked the errors derived from different sampling strategies such as cross-front and along-front samplings. In our work we proceed in a similar way to the experiments designed by Allen et al. (2001) and Rixen et al. (2003): we use a modelled time sequence of fields representing unstable baroclinic waves, from which we extract the observations that would result from different realistic sampling strategies. All data sets are processed as if they were actual observations in order to produce gridded fields of both observed variables (dynamic height) and derived variables (relative vorticity, vertical velocity and dynamic height tendency). The differences between the fields obtained from the simulated oceanographic cruises and the model fields (the ‘truth’) will give a quantitative estimate of the impact of the lack of synopticity. An ideal synoptic cruise consisting of the same number of stations will be used as the control case, as it will involve errors derived from the discrete sampling but not synopticity errors.

However, the aim of this work goes beyond the evaluation of synopticity errors: we also propose and test two methods aimed at mitigating the impact of the lack of synopticity. A first method is based on the QG tendency equation (see for instance Holton, 1992) which, unlike its counterpart the omega equation, has not received much attention in the oceanographic literature. Namely, the local time evolution given by the tendency equation is used to project observation values onto a common time (e.g., the central time of the sampling period). The resulting ‘pseudo-synoptic’ observations are re-analyzed and the new gridded fields compared to model fields in order to evaluate the improvement.

The second method combines the relocation of stations and the correction of observations. Station relocation methods are not new: Rixen et al. (2001) suggested a method based on the idea of relocating stations so as to represent a ‘pseudo-synoptic’ distribution of observation points. The difference is that Rixen’s method is based on the advection of water parcels by the geostrophic velocity, so that stations are relocated even in the case of dynamically stationary fields. This might be appropriate for some conserved

quantities such as biochemical parameters. For dynamical parameters, however, the increase of interpolation errors that derives from the strong spatial distortion of the data set (e.g., profiles are no longer vertical, as the geostrophic velocity varies with depth) may eventually be larger than the synopticity errors intended to be corrected.

The station relocation proposed in this work is based on the computation of a ‘system velocity’, i.e., the speed at which the sampled pattern is moving across the domain. This speed would be zero in the case of stationary fields and would be equal to the phase speed in the case of propagating waves. In other cases, however, the definition of a homogeneous system velocity may be more problematic, in which case the correction method proposed by Rixen et al. (2001) may be more convenient. A first method to compute such a system velocity has been proposed by Hoskins et al. (2003), though not for the purpose of station relocation. A second method has been suggested by Pascual et al. (2004), who also proposed to relocate the stations in order to mitigate the impact of the lack of synopticity. In our work, in addition to the station relocation we also propose to correct the observations basing on the estimation of a growth rate, an aspect that was not considered in the work by Pascual et al. (2004).

The structure of the paper is as follows. Section 2 is devoted to describe the simulated fields and the different sampling strategies. Next (section 3), errors resulting from simulated non-synoptic cruises are evaluated. In section 4 we summarize the theoretical basis of the proposed correction methods and give the details of their practical implementation. Results from the application of the methods are presented in section 5 and discussed in section 6. Conclusions are also outlined at the end of section 6.

2. THE DATA SET

The effects of the lack of synopticity are strongly case-to-case dependent, and therefore it is not possible to obtain a general rule for the errors involved in the recovery of observed fields. Our option in this work is to focus on a simple case from which the basis of the problem can be investigated. This was the aim of Allen et al. (2001) and Rixen et al. (2003), who used mesoscale numerical models to simulated a ‘true’ field consisting of eastwards-propagating unstable baroclinic waves. We operated in a similar way except that we wanted to exactly control the propagation speed and growth rate of the waves. With this

aim, a single mode was represented using the analytical model of baroclinic instability proposed by Tang (1975). The limitations of our approach with respect to the application of the method to a real data set will be discussed in the last section. In the following we give the details on the modelled fields and the simulated samplings.

2.1 The ‘true’ dynamical fields

Tang's model is quasi-geostrophic, and therefore it must be considered a simplified view of actual fields. However, diagnostic studies undertaken under the QG framework usually give realistic results, provided they focus on scales larger than the Rossby radius of deformation. Hence, QG is probably less limiting than the assumption of a single propagation mode, regarding the representation of actual fields.

Tang's model assumes an upper layer of depth H_1 with Brunt-Väisälä frequency N_1 , maximum (surface) current speed U and constant shear U/H_1 over a quiescent lower layer extending down to a depth H_2 with Brunt-Väisälä frequency N_2 . Despite the simplicity of the model, it usually provides realistic values for the propagation speed and growth rates of the modes. In our particular case, the input parameters were those characterizing frontal structures observed in the Western Mediterranean, which are typical of shelf-edge fronts observed in many regions. Namely, we set $H_1=300$ m, $N_1=5 \cdot 10^{-3} \text{ s}^{-1}$, $U=30$ cm/s, $H_2=600$ m and $N_2=8 \cdot 10^{-4} \text{ s}^{-1}$. We focused on a mode of 90 km wavelength developing in a jet about 45 km wide in the cross-frontal direction. For the quoted input parameters, Tang's analytical model predicts a downstream propagation speed of 8.0 km/day for this mode and a growth with an e-folding time of 4.6 days.

The sequence of dynamic height fields was projected onto a 2 km x2 km grid covering a 56 km x136 km domain. Some snapshots of the dynamic height field at 100 m depth (a level that is representative of the upper layer dynamics) are shown in Figs. 1a-b and 2a. In particular, we centered our attention at day 13 of the sequence: the geostrophic relative vorticity, vertical velocity and tendency fields computed from model gridded data are also shown in Fig. 2. Relative vorticity (Fig. 2b) was directly computed from dynamic height (Fig. 2a), the obtained values being within the range $\pm 1.6 \cdot 10^{-5} \text{ s}^{-1}$ (e.g., ± 0.16 f at middle latitudes). The computation of the vertical velocity and tendency fields deserves more attention.

Vertical velocities were obtained by integrating the QG omega equation on an f-plane, as described in Part I of this work. The equation was integrated setting $w=0$ at the upper and lower boundaries and also at the along-front boundaries, since the modeled waves are confined to the model domain in the cross-frontal direction. At the upstream and downstream boundaries it was the normal derivative of w that was set to zero (for a detailed description of the method see Pinot et al. 1996). The obtained values are within the range ± 18 m/day (Fig. 2c), which are typical values for frontal mesoscale structures.

In the framework of QG dynamics, the equation complementary to the omega equation is the so called tendency equation (Holton, 1992). It is a linear partial differential equation formally very similar to the omega equation, but for the unknown χ , where χ is the local time derivative ($\partial\phi/\partial t$) of dynamic height ϕ . As for the omega equation, the forcing term is related to the distributions of vorticity and thickness advection and therefore it can be computed from dynamic height alone (i.e., without explicitly determining the distribution of w ; see Pascual et al. (2004) for more details). The most important formal difference with respect to the omega equation is that χ cannot be set to zero at surface. From the QG density conservation equation it can be shown that a surface boundary condition consistent with setting $w=0$ is $\partial\chi/\partial z|_s = (g/\rho)v_g \cdot \nabla_h \rho$. The other boundary conditions can be set in the same way as for the omega equation.

The obtained values are within the range of ± 0.9 dyn cm/day (Fig. 2d). Most important, the regions of positive/negative tendency are neither collocated with dynamic height ridges/troughs (which would be the case for standing growing waves) nor exactly located in between them (which would be the case for a propagating neutral mode). As such, the QG tendency field reflects the actual tendency of a propagating growing mode.

Because it will be crucial for the correction methods tested later on, we will further check the accuracy of the tendency field. The errors associated with the computation method itself (e.g., those derived from the numerical integration of the tendency equation, in particular from the boundary conditions, but without the handicaps of the discrete sampling or the lack of synopticity) can be evaluated by comparing the result of applying the tendency equation to model grid data (Fig. 2d) with the actual model tendency (Fig. 1c). The latter was computed at day 13 simply as the difference between dynamic height at days 13.5 and 12.5 divided by a 1 day time lag.

As expected, the QG tendency gives an overall good representation of the actual tendency, though with some distortion in the field pattern. In Part I of this work we stated that when sampled structures are smaller than the size of the domain, the ellipticity of the omega and tendency equations makes the interior solution relatively insensitive to the imposed conditions except at the few grid points closer to the boundaries. However the structures simulated in this work are not much smaller than the domain, and therefore the observed distortion is likely related to boundary conditions (a similar distortion is actually observed for the vertical velocity field, Fig. 2c). The mean difference between the two fields is 0.057 dyn.cm/day, roughly a 10% of the tendency field standard deviation (0.562 dyn.cm/day). As it will be shown later on, these errors are significantly smaller than those derived from the lack of synopticity, so that in the framework of this work the computation method can be considered as reasonably accurate.

2.2 The simulated samplings

Four different samplings of the ‘true’ field were considered. They all consisted of 8x18 stations separated 8 km in both horizontal directions (so that they cover the whole model domain), which can be considered representative of oceanographic cruises focusing on mesoscale dynamics. Simulated profiles spanned the whole vertical domain and no instrumental error was considered. This is justified by the results obtained in Part I of this work, which showed that for derived variables inferred from typical CTD surveys, the impact of observation errors is smaller than the impact of the discrete sampling.

The differences between the samplings were that:

- i) For the first one (hereafter referred to as the ‘synoptic sampling’) no time lag between stations was considered. That is, all values taken as observations correspond to day 13 00 h model fields sampled at station points.
- ii) For the second sampling, a 1 hour time lag was assumed in between stations. This value was determined assuming a navigation speed of about 8.5 knots (i.e., about half an hour navigation between stations) and that the operations to sonde a 600 m water column can take another half an hour. Under these conditions it would take 6 days to sample the whole domain, a period that was centred at 00h of day 13 of the model sequence (i.e., the first station value corresponds to 01h of day 10 and the last one to 00 h of day 16). The first station was located at the lower-left (upstream) corner of the domain and the

sampling strategy was the typical cross-frontal saw-tooth track sweeping the domain downstream. Following the described sampling strategy the domain is covered at a rate of about 23 km/day (i.e., about three times the wave speed) in the direction of the wave propagation. This sampling will be hereafter referred to as the ‘downstream sampling’.

- iii) The third sampling was exactly the same as the second one except in that the first station was located at the lower-right (downstream) corner of the domain and the cross-frontal saw-tooth track was taken sweeping the domain upstream. Hence, this sampling will hereafter be referred to as the ‘upstream sampling’.
- iv) Finally, the fourth sampling strategy was an along-front saw-tooth track consisting of alternate upstream-downstream legs starting at the lower-left corner of the domain. This sampling will hereafter be referred to as the ‘along-front sampling’.

3. EVALUATION OF ERRORS DERIVED FROM NON-SYNOPTIC SAMPLINGS

3.1 *Observed variables*

The four sets of synthetic dynamic height observations were subjected to the same data processing. Firstly, they were interpolated onto the model grid using the Optimal Statistical Interpolation (hereafter OI) scheme described in Part I. The parameters were also the same, as the waves modeled here roughly correspond to a gaussian correlation scale with a characteristic scale of 15 km. Since the simulated fields do not contain small-scale structures, no additional filtering would be required. However, we wanted the analysis to include also a negative aspect of the filtering applied when dealing with actual data, namely the larger penetration of boundary effects inside the domain (see Part I). Therefore we convoluted the OI analysis with a normal-error filter, setting the cut-off wavelength to 32 km (four times the separation between stations).

Results for the four surveys are shown in Figs. 3a, 4a, 5a and 6a respectively, and the rms differences with respect to the model fields are listed in Table 1 (all them correspond to 100 m depth). As expected, the synoptic cruise reproduces the original field rather accurately. Rms differences are about 0.07 dyn cm, which represents a fractional error of about 4% with respect to the field standard deviation (1.86 dyn cm). This value is in between the errors predicted in Part I of this work for a SeaSoar sampling (2%) and a 10

km spaced CTD sampling (6%). [When comparing the values obtained in the two parts, it is worth reminding that in Part I they were predicted by the OI formulation, which implicitly assumes that the fields exactly obey the correlation statistics (something which is not exactly true in practice). On the other hand, errors derived in Part I include the (small) contribution of observation errors, which have not considered in the simulations of Part II.]

Worse results are obtained for the downstream and upstream samplings. The wave structure of the true field is significantly stretched in the first (Fig. 4a) and compressed in the second (Fig. 5a). Additionally, the growing of the waves reflects in smaller/larger wave amplitudes in those sectors of the domain sampled in the early/latter stages of the cruises. Rms differences are about 0.67-0.68 dyn cm (36% fractional error), which already suggests that the impact of the lack of synopticity can be much more important than the impact of observation errors or that derived from a reasonable discrete sampling.

For the along-front sampling, the most evident feature is the cross-frontal tilting of structures (Fig. 6a). This is an expected consequence of the time lag between the sampling of the lower and upper sectors of the domain, as the wave propagates downstream during the sampling period. Rms differences with respect to the model field are however significantly smaller than for the upstream and downstream cruises: about 0.28 dyn cm (15% fractional error). The benefits of an along-front sampling were already reported by Rixen et al (2003), who carried out a similar experiment.

3.2 Derived variables

The relative vorticity, vertical velocity and tendency fields were computed from gridded dynamic height fields in the same way as the model fields (see section 2.1). Results for the four surveys are shown in Figs. 3b-d, to 6b-d; they are qualitatively similar to those obtained by Rixen et al. (2003) and therefore we will focus the description on the rms differences with respect to model fields (listed in Table 1). The synoptic cruise (Figs. 3b-d) reproduces rather faithfully the original patterns (Figs. 2b-d), though maxima and minima appear slightly smoothed in all fields. The fractional errors are of the order of 7% for relative vorticity, and about 7.5% for the vertical velocity and tendency fields. These error values are again in between the inner-domain errors predicted in Part I for a SeaSoar sampling (5%) and a 10 km spaced CTD sampling (15%).

The downstream and upstream samplings (Figs. 4b-d, 5b-d) show the typical stretched/compressed patterns, with the maximum and minimum values significantly reduced/enhanced as a consequence of the stretching/compression of the dynamic height field. For relative vorticity, fractional errors are about 65% and 91% for the downstream and upstream samplings respectively; for the vertical velocity they are 82% and 115%; and for the tendency field they are 82% and 96%. It seems, therefore, that the tendency field is not more handicapped than the vertical velocity, despite the surface boundary condition of the first (the horizontal advection of density) is surely distorted, while it is not for the second (for which $w=0$ is always assumed).

For the along-front sampling (Figs. 6b-d), the cross-frontal tilting of structures is more apparent in the derived variables than in the dynamic height field. Maxima and minima appear shifted upwards or downwards across the front, but their values are more accurate than for the downstream and upstream samplings. Fractional errors computed for this sampling were about 73% for the relative vorticity, 58% for the vertical velocity and 56% for the tendency field.

4. METHODS AIMED AT THE MITIGATION OF SYNOPTICITY ERRORS

At least part of the striking impact of the lack of synopticity can possibly be reduced through some kind of correction applied either to the station position or to the observation values. Two methods are proposed in the following.

4.1 Observation correction based on the QG tendency equation

The simplest method would be using the tendency field to substitute the original dynamic height values ‘observed’ at station ‘i’ and time t_i [$\phi_i(t_i)$] by those that would be measured at the same location but at a reference time t_0 common to all stations [$\phi^*_i(t_0)$]. This implies estimating the tendency at station points [χ_i] (e.g. via bilinear interpolation from the gridded tendency values) and, most importantly, assuming that the tendency remains constant during the time lag between t_i and t_0 . It is also implicitly assumed that the distortion of the tendency field due to the non-synoptic sampling is not so severe that it worsens the synopticity of observations rather than improves it. Both assumptions are

rather strong and must be kept in mind when discussing results. Following this approach, the set of ‘pseudo-synoptic’ observations $[\phi_i^*(t_0)]$ can be simply obtained as

$$\phi_i^*(t_0) \approx \phi_i(t_i) + (\chi_i) \cdot (t_0 - t_i) \quad (1)$$

The advantages of the method are its simplicity and that it is independent of the sampled pattern. That is, it can be applied to any dynamical situation, as no assumption is made apart from the validity of QG. A disadvantage is that only dynamic height and subsequently derived variables can be corrected. The density field can be inferred from the corrected dynamic height field, but the temperature and salinity fields cannot.

4.2 Station relocation and observation correction based on a system velocity

The first step of this method (the station relocation) has recently been proposed by Pascual et al. (2004). It is based on the assumption that the sampled pattern propagates at a constant speed $\mathbf{c}=(c_x, c_y)$ across the domain. As stated above, this will be reasonably true in the presence of waves embedded in a front, as the ones modelled here, or in the case of a single moving eddy. However, it will clearly not be appropriate for large domains where different structures can evolve in rather different ways. On the other hand, the method allows the correction of any variable, as it works on the station position and not on observed values.

The method operates as follows: the original station locations (x_i, y_i) are changed to the positions (x_i^*, y_i^*) that they would occupy at a common reference time t_0 if they were moving with speed \mathbf{c} . It is worth recalling here that \mathbf{c} is a unique ‘system velocity’ and not water parcel local velocities (approximated by geostrophic velocities in Rixen et al., 2001). This is easily achieved doing

$$\begin{aligned} x_i^*(t_0) &\approx x_i + c_x(t_0 - t_i) \\ y_i^*(t_0) &\approx y_i + c_y(t_0 - t_i) \end{aligned} \quad (2)$$

The system velocity can be computed from the tendency field as proposed by Pascual et al. (2004). The method is summarized in the Appendix for the sake of completeness. For the single-mode waves simulated in this work, the system velocity should fit the real part of the wave phase speed. In the case of more realistic, multi-modal instabilities, the system velocity is expected to reflect the mean propagation speed of the perturbations.

The station relocation is intended to correct the lack of synopticity derived from the propagation of structures. However, the eventual growing or decaying of structures is not accounted for by this method. We therefore propose to go beyond the relocation and also correct the station values based on the estimation of a growth rate. It can be demonstrated that for exponentially growing or decaying waves (with amplitudes denoted by $A_0 \exp[\gamma t]$), the e-folding time γ^{-1} can be obtained from the covariance $\langle \chi \phi \rangle$ between the dynamic height and tendency fields,

$$\gamma^{-1} = \sigma_{\phi}^2 / \langle \chi \phi \rangle \quad (3)$$

where $\sigma_{\phi}^2 = \langle \phi^2 \rangle$ is the dynamic height anomaly variance. Thus, in the case of propagating neutral modes, the maxima and minima of the tendency field are located in between ridges and troughs of dynamic height, so that $\langle \chi \phi \rangle = 0$ and $\gamma^{-1} = \infty$. The opposite case would be a standing wave, for which maxima and minima of the tendency field exactly coincide with ridges and troughs of dynamic height, so that $\langle \chi \phi \rangle = \sigma_{\phi} \sigma_{\chi}$ and therefore $\gamma^{-1} = \sigma_{\phi} / \sigma_{\chi}$ (where $\sigma_{\chi}^2 = \langle \chi^2 \rangle$ is the tendency field variance).

In the atmosphere, the tendency field is usually dominated by the propagation of structures (Carlson, 1991) to the point that it can be difficult to identify the contribution due to their growing/decaying. Although it is not clear that the same applies to the ocean, in practice we found that the values of the e-folding obtained from (3) were not accurate. To overcome this problem, the contribution due to propagation χ_p can be subtracted from the total tendency, so that the remaining contribution $\chi_g = \chi - \chi_p$ will better reflect the growing (as well as to other effects, see the Appendix for details). Since in principle $\langle \chi_p \phi \rangle \approx 0$, the growth rate γ^{-1} can be obtained by using χ_g in place of χ in (3).

5. RESULTS

The results of applying the two proposed methods to the downstream, upstream and along-front samplings are shown in Figs. 7-9 and 10-12 respectively, and the error statistics are given in Table 1. In the following we comment the results of each method in two separate sections.

5.1 Correction method based on the QG tendency equation

For the downstream and upstream cruises, this method only yields a small reduction of the errors derived from the lack of synopticity (see Table 1). The main problem is that the tendency fields inferred from the non-synoptic observations are too distorted to provide an accurate correction. For the downstream cruise, for instance, dynamic height (Fig. 7a) is clearly less stretched than it was before the correction (Fig. 4a), but it is still far from approaching the true shape (Fig. 2a). In the same way, the gradients of the corrected upstream cruise (Fig. 8a) are still sharper than true gradients. The consequences on the relative vorticity (Figs. 7b and 8b) and vertical velocity (Figs. 7c and 8c) are obvious: in addition to the remaining stretching/compression of structures, maximum and minimum values are still significantly smoothed/enhanced. It is perhaps more important to note that the corrected tendency fields (Figs. 7d and 8d) are still clearly distorted. This prevents from applying the method in an iterative way, i.e., using the corrected tendency fields (instead of those initially retrieved) for a further correction attempt.

The method works significantly better for the along-front sampling. The cross-frontal tilting of structures has been reduced, though it is still apparent in the corrected fields (Fig. 9). Rms differences, which for non corrected samplings were already lower for the along-front cruise than for the downstream and upstream cruises, are significantly reduced by the correction method: from 15% to 7% for dynamic height, from 73% to 32% for relative vorticity and from 58% to 30% for the vertical velocity. The better performance for the along-front sampling must be associated with the better accuracy of the retrieved tendency field: tendency fractional errors were about 56% for the along-front sampling, while they were 82% and 96% for the downstream and upstream samplings.

5.2 Correction method based on a system velocity

Prior to the application of this method, we computed the system velocity and the growth rate (expressed as an e-folding time) from the model fields and from the synoptic cruise. In both cases the estimations based on the tendency equation (see the Appendix) yielded rather accurate values: 7.7 km/day and 4.4-5.4 days, compared to the actual values 8.0 km/day and 4.6 days (see Table 2).

Instead, the values obtained for the three realistic sampling strategies were rather different. As expected, a too low system velocity (4.9 km/day) and a too large e-folding

time (> 8 days) were obtained from the downstream cruise as a consequence of the stretched pattern. Conversely, a larger system velocity (8.8 km/day) and a smaller e-folding time (< 4 days) were obtained for the upstream cruise, though in this case the values were more accurate than for the downstream cruise. The along-front cruise was the one yielding the best results: 7.4 km/day and 4.6-5.8 days.

The correction method, was implemented in two steps, in order to distinguish between the benefits of the station relocation and of the observation correction. In a first step, only the station relocation was applied; in a second one, relocated observations were corrected basing on the estimated growth rate. Rms differences between the results produced by each of the two steps and the model fields are listed in Table 1.

Except for a single field (the dynamic height of the downstream sampling), the station relocation by itself results in a larger error reduction than the correction method tested in the previous section. This is particularly true for the upstream sampling, for which errors reduce to about 1/3 of initial errors. However, initial errors were particular large for that sampling, so that in absolute terms, the cruise resulting in the smallest errors after applying the correction is again the along-front one (fractional errors of 7%, 31%, 25% and 22% for dynamic height, relative vorticity, vertical velocity and tendency, respectively), closely followed by the upstream cruise (9%, 22%, 28% and 34% fractional errors). The downstream cruise is by far the one with largest errors (32%, 49%, 58% and 48%).

When applying the correction of observations, results for the along-front and upstream samplings are further improved (also for the downstream sampling, but to a lesser extent). The best case is definitely the along-front sampling, for which errors reduce to 5%, 8.5%, 7% and 7.5% for dynamic height, relative vorticity, vertical velocity and tendency, respectively. It is worth recalling here that fractional errors for the synoptic cruise were 4%, 7%, 7.5% and 7.5%, so that synopticity errors are almost completely eliminated by the method. This is also evident when looking at the corrected fields (Fig. 12): they just show a very slight cross-frontal tilting, and the maxima and minima show the same slight smoothing with respect to the model fields as the synoptic sampling (Fig. 3).

For the upstream sampling the method also eliminates most synopticity errors (see Table 1). However, Fig. 11 shows that because of the station relocation, the sampled domain has considerably enlarged: the 18 station legs originally separated 8 km (spanning

a 136 km domain in the along-front direction) are now separated about 11 km and therefore span a 187 km domain (only the inner part of it is shown in Fig. 11). For the downstream sampling the remaining errors are between 1/3 and 1/2 of the original synopticity errors, and are mostly associated with smoothing in the upstream sector of the domain (Fig. 10). This Figure also shows the reduction of the sampled domain after relocation (the legs are now separated 6.5 km in the along-front direction, spanning a domain of about 110 km).

A main reason for the success of the along-front sampling must be attributed to the fairly accurate representation of the dynamic height and tendency fields already in the first step, since the phase speed and growth rate critically depend on these two fields. The upper limit of the benefits provided by the method can be evaluated by using the true values of the phase speed and the growth rate (which are unknown in practice) instead of those computed from the recovered fields. Results indicate that errors might be further reduced only for the downstream case (though there is no warranty for the converge of results). Instead, the errors of the upstream and along-front cruises were only slightly reduced, which indicates that for both sampling strategies a single iteration of the correction method might be enough to get close to the expected maximum error reduction.

6. DISCUSSION AND CONCLUSIONS

Three realistic sampling strategies have been tested to evaluate the impact of the lack of synopticity on dynamical fields. In the best case (the along-front sampling), fractional errors are of the order of 15% for dynamic height, and more than 50% for relative vorticity, vertical velocity and the tendency field. These values are much larger than those obtained in Part I of this work for observation and sampling errors (about 2-6% for dynamic height and 5-15% for relative vorticity and vertical velocity, all them referred to an inner domain). Hence, a first conclusion is that the lack of synopticity of observations can be, by far, the most important error source in the presence of structures like those examined in this work.

Of the two correction methods aimed at mitigating synopticity errors, the first one (based on the use of the tendency field to correct observations) has the advantage of being independent of the sampled pattern, and the disadvantage that only dynamic height and subsequently derived variables can be corrected (i.e., the temperature and salinity fields

cannot). An additional handicap inferred from the test is that the method is quite sensitive to the initial recovery of the tendency field. This is why the correction applied to the downstream and upstream samplings has not been very effective. For the along-front cruise, however, errors have been reduced down to 7% for dynamic height and between 32-34% for relative vorticity, vertical velocity and the tendency field.

The second method (based on the relocation of stations to compensate for the propagation and on the correction of observations to compensate for the growing) assumes that the whole sampled pattern propagates at a constant speed across the domain. Results have shown that also this method is sensitive to the initially recovered fields. However, since the along-front sampling is able to recover the fields without too much distortion, synopticity errors have been almost completely eliminated for that sampling strategy.

A second conclusion, therefore, is that the along-front sampling is definitely the most appropriate one for this type of ocean disturbances. The fields are not only better recovered than for the other samplings (as already demonstrated by Rixen et al., 2003), but also (and actually as a consequence of this) the proposed correction methods are much more effective for this sampling strategies. It is also worth noting that when the proposed station relocation is applied to the along-front sampling, the effectively sampled domain is similar to the original domain. This does not happen for the upstream/downstream samplings, for which the domain is significantly stretched/compressed after relocation.

For the case analyzed in this work, the second correction method gives better results than the first. A likely reason is that for the first method to be successful, it requires the tendency field to be accurate at any point. On the other hand, the second method is based on the estimation of ‘mean’ properties (namely, the system phase speed and the growth rate), and it is therefore more robust in the presence of local errors in the tendency field. As far as these mean properties are representative of the whole domain, the second method will likely produce better results. Regarding the two steps of the second method, the station relocation by itself is effective in reducing the deformation of the fields derived from the propagation of structures. However, a significant further error reduction can be achieved when observations are corrected on the basis of a growth rate. Because the estimation of this growth parameter has a larger amount of uncertainty than the system velocity, it might be advisable to apply this second step only when the growing/decaying

of structures is well apparent. This can be checked comparing the shapes of (or computing the correlation between) the dynamic height and tendency fields.

Finally, some comments are to be made on the practical significance of the proposed correction methods; in particular on their application to more realistic fields and also on the extent to which other authors can be convinced about using them. Regarding the first item, we can firstly state that the simulated single-mode instabilities have been useful to investigate the basis of the problem. Actual oceanographic fields are obviously more complex than those simulated here, but it is also true that examining particular, more complex cases will not necessarily produce more general hints on the performance of the methods. On the other hand, we must recognize some limitations in the practical application of the proposed methods. The relocation of stations, for instance, should only be applied when there are evidences of the existence of a more or less homogeneous system velocity (e.g., propagation of waves embedded on a front or the propagation of isolated structures). In such cases, the method is expected to yield a remarkable benefit, though it cannot be pretended to completely eliminate synopticity errors as in this work. An example of the application of the method to a real case is given in Pascual et al. (2004), though in that case the results were not compared with the (unknown) true fields.

A limitation shared by both methods is that the tendency field must be at least fairly recovered by the initial interpolation. However, it has been shown that even for fields as distorted as those recovered by the upstream or downstream sampling, the correction methods improve the first estimate. And when the initial fields are fairly recovered, as for along-front cruise, the methods yield a quite accurate representation. More precisely, they turn a case in which synopticity errors are several times larger than the contribution of observation and sampling errors (evaluated in Part I of this work) into a case in which synopticity errors are smaller than the other error sources.

Regarding the practical implementation of the correction methods, we are aware that both (but mainly the second one) involve a significant degree of analysis. This is clearly a handicap in front of more simple methods like the one by Rixen et al. (2001). Our opinion is that Rixen's method and those proposed here are somehow complementary. The first is simpler, but, it can hardly be applied to a situation like the one represented in this work: with geostrophic velocities of the order of 40 cm/s (i.e., about 35 km/day) and a 6 day long cruise, the station relocation would surely have a negative impact on the recovery

of the fields. Therefore, Rixen's method will be appropriate for short cruises (e.g., SeaSoar cruises in small domains). The methods proposed here are more complex, but regarding the duration of the cruises, they have a larger range of applicability. As stated above, the main limitation, affecting only the second method, is the existence of a more or less homogenous system velocity, but this is fairly true for a variety of situations.

ACKNOWLEDGMENTS

This research has been undertaken in the framework of the BIOMEGA project (REN2002-04044-C02-01/MAR) funded by the Spanish Marine Science and Technology Program. Ananda Pascual acknowledges a Marie Curie Host Industry Fellowship funded by the European Commission (Fellowship Contract: HPMT-CT-2001-00100). We are very grateful to Prof. Robert L. Haney for his thoughtful comments.

APPENDIX: ESTIMATION OF THE 'SYSTEM' PROPAGATION VELOCITY

Following Pascual et al. (2004), the computation of the system velocity is based on the relationship between a local time derivative observed from a fixed reference ($\partial\phi/\partial t = \chi$) and one observed from a frame of reference moving with speed \mathbf{c} ($\partial\phi/\partial t|_{\mathbf{c}}$):

$$\partial\phi/\partial t|_{\mathbf{c}} = \chi + \mathbf{c} \cdot \nabla_h \phi \quad \square\square\square\square(A1)$$

Expression (A1) is obviously valid for any variable ϕ , but here it will be applied to dynamic height, so that ($\partial\phi/\partial t = \chi$) will be the dynamic height tendency.

Assuming that local variations are mainly due to the structure propagation (rather than the structure growing/decaying), the term ($\partial\phi/\partial t|_{\mathbf{c}}$) will be minimized when the speed \mathbf{c} approaches the propagation speed of the sampled structure (for an ideal pattern propagating exactly with \mathbf{c} without growing or decaying, term $\partial\phi/\partial t|_{\mathbf{c}}$ would be exactly equal to zero). Hence, the problem of finding \mathbf{c} reduces to the minimization of a cost function $J(\mathbf{c}) = \sum_i (\chi + \mathbf{c} \cdot \nabla_h \phi)^2$, which can be solved imposing $\partial J(\mathbf{c})/\partial c_x = 0$ and $\partial J(\mathbf{c})/\partial c_y = 0$. It then results:

$$\begin{pmatrix} \sum_i \phi_x^2 & \sum_i \phi_x \phi_y \\ \sum_i \phi_x \phi_y & \sum_i \phi_y^2 \end{pmatrix} \begin{pmatrix} \mathbf{c}_x \\ \mathbf{c}_y \end{pmatrix} = \begin{pmatrix} -\sum_i \chi \phi_x \\ -\sum_i \chi \phi_y \end{pmatrix} \quad (\text{A2})$$

where \sum_i extends to all grid point values of the selected domain and ϕ_x, ϕ_y denote $\partial\phi/\partial x, \partial\phi/\partial y$, respectively. Obtaining (c_x, c_y) from the gridded fields of dynamic height and tendency is then straightforward from (A2).

Once \mathbf{c} is obtained, the term $\partial\phi/\partial\mathbf{t}|_{\mathbf{c}}$ can be readily evaluated by means of (A1). Comparing the variance of this term relative to the tendency variance will give an estimate of which fraction of the later cannot be associated with the propagation of the structures. This remaining variance can in principle be associated with growing/decaying effects (though in practice it could also be due to the presence of structures moving with different speeds). Therefore, we can assume that $\partial\phi/\partial\mathbf{t}|_{\mathbf{c}}$ accounts for the growing/decaying contribution of the tendency field referred in section 4.2 as $[\chi_g]$.

In a different context, Hoskins et al. (2003) proposed to compute a system velocity \mathbf{c} based on the density conservation equation. When this is written in a frame of reference moving with speed \mathbf{c} , it becomes:

$$\partial \rho / \partial t \big|_c = -(\mathbf{V}_g - \mathbf{c}) \cdot \nabla_h \rho - w \partial \rho / \partial z = [-\mathbf{V}_g \cdot \nabla_h \rho - w \partial \rho / \partial z] + \mathbf{c} \cdot \nabla_h \rho \quad (A3)$$

Expression (A3) is formally equivalent to (A1), which was the starting point of the method based on the tendency equation. The problem of finding \mathbf{c} can therefore be solved in the same way. The difference with respect to the previous method is that (A3) requires knowledge of the vertical velocity field, instead of the tendency field.

REFERENCES

- Allen, J. T., J. F. Read, S. G. Alderson, H. Desai, 1992: SeaSoar and CTD sections across the Iceland-Faeroes and Faeroes Shetland Channel, August 1990. *IOSDL Report* 295, Southampton Oceanography Centre.
- Allen, J. T., D. A. Smeed, A. J. Nurser, J. W. Zhang, M. Rixen, 2001: Diagnosis of vertical velocities with the QG omega equation: an examination of the errors due to sampling strategy. *Deep-Sea Res.* 48, 315-346.
- Carlson, T, 1991: *Mid-latitude Weather Systems*. HarperCollins Academic, London.
- Gomis, D., S. Ruiz, M. A. Pedder, 2001: Diagnostic analysis of the 3D ageostrophic circulation from a Multivariate Spatial Interpolation of CTD and ADCP data. *Deep Sea Res. I*, **48**, 269-295.
- Holton, J. R., 1992: *An introduction to dynamic meteorology*. Academic Press, San Diego.
- Hoskins, B., M. A. Pedder, D. W. Jones, 2003: The omega equation and potential vorticity. *Quart. J. Roy. Met. Soc.*, **129B**, 3277-3304.
- Joyce, T. M., 1989: On in situ "calibration" of shipboard ADCPs. *J. Atmos. Ocean Tech.*, **6**, 169-172.
- Matthews, P. A., 1997: The impact of non synoptic sampling on mesoscale oceanographic surveys with towed instruments. *J. Atmos. Ocean Tech.*, **14**, 162-174.
- Pascual, A., D. Gomis, R. L. Haney, S. Ruiz, 2004: A quasi-geostrophic analysis of a meander in the Palamós Canyon: vertical velocity, geopotential tendency and a relocation technique. *J. Phys. Ocean.*, **34**, 2274-2287.
- Pinot, J. M., J. Tintoré, D. P. Wang, 1996: A study of the omega equation for diagnosing vertical motions at ocean fronts. *J. Mar. Res.*, **54**, 239-259.
- Pollard, R. 1986. Frontal surveys with a towed profiling conductivity/temperature/depth measurements package (SeaSoar). *Nature*, **323**, 433-435.
- Rixen, M., Beckers, J.-M., J. T. Allen, 2001: Diagnosing vertical velocities using the QG omega equation: a relocation method to obtain pseudo-synoptic data sets. *Deep-Sea Res.*, **48**, 1347-1373.

- Rixen, M., J. T. Allen, S. Alderson, V. Cornell, N. Crisp, S. Fielding, A. T. Mustard, R. T. Pollard, E. E. Popova, D. A. Smeed, M. A. Srokosz, 2003: Along or across front ocean survey strategy ?. An operational example at an unstable front. *Geophys. Res. Let.*, **30**, NO. 1, 1017, doi: 10.1029/2002GL015341,2003.
- Tang, C., 1975: Baroclinic instability of stratified shear flow in the ocean and atmosphere. *J. Geophys. Res.*, **80**, 1168-1175.

FIGURE CAPTIONS

Figure 1: sequence of dynamic height fields (dyn cm) representing an unstable baroclinic mode of 90 km wavelength embedded in a 45 km wide jet, as given by the Tang model. They correspond to days 10 (a) and day 16 (b) of the sequence (day 13 is shown in Fig. 2). (c) Dynamic height tendency (in dyn cm/day) at day 13. All the fields of this and the following figures correspond to 100 m depth (a level that is representative of the upper layer dynamics); only the inner part of the 136x56 km² model domain is shown.

Figure 2: (a) Model dynamic height (dyn cm) at day 13. (b) Relative vorticity (10^{-5} s^{-1}), (c) QG vertical velocity (m/day) and (d) QG tendency (dyn cm/day) computed from the 3D model dynamic height at day 13.

Figure 3: Results for the synoptic sampling: (a) dynamic height (dyn cm), (b) relative vorticity (10^{-5} s^{-1}), (c) QG vertical velocity (m/day) and (d) QG tendency (dyn cm/day). The position of 96 stations has been overlapped in (a) (other 48 stations are located beyond the boundaries of the represented inner domain).

Figure 4: As in Fig. 3, but for the downstream cruise.

Figure 5: As in Fig. 3, but for the upstream cruise.

Figure 6: As in Fig. 3, but for the along-front cruise.

Figure 7: Results for the downstream cruise: (a) dynamic height (dyn cm), (b) relative vorticity (10^{-5} s^{-1}), (c) QG vertical velocity (m/day) and (d) QG tendency (dyn cm/day) obtained from the ‘pseudo-synoptic’ observations corrected following the tendency method.

Figure 8: As in Fig. 7, but for the upstream cruise. Note that in panels b-d the spacing between isolines has changed with respect to the other figures.

Figure 9: As in Fig. 7, but for the along-front cruise.

Figure 10: Results for the downstream cruise: (a) dynamic height (dyn cm), (b) relative vorticity (10^{-5} s^{-1}), (c) QG vertical velocity (m/day) and (d) QG tendency (dyn cm/day) obtained from the ‘pseudo-synoptic’ relocated stations with observations corrected on the basis of the estimated growth rate. The position of the relocated stations has been overlapped in (a).

Figure 11: As in Fig. 10, but for the upstream cruise.

Figure 12: As in Fig. 10, but for the along-front cruise.

TABLES

	Dynamic Height (dyn cm)	Geostr. Relative vorticity (10^{-5}s^{-1})	QG vertical velocity (m/day)	QG Tendency (dyn cm/day)
Incr. field standard deviation	1.862	1.003	10.37	0.562
Synoptic cruise rms error	0.073 (3.9)	0.069 (6.9)	0.78 (7.6)	0.041 (7.3)
Downstream cruise rms error	0.671 (36.0)	0.648 (64.6)	8.54 (82.4)	0.461 (82.0)
Error after tendency correction	0.555 (29.8)	0.493 (49.2)	6.49 (62.6)	0.392 (69.8)
Error after relocation	0.586 (31.5)	0.490 (48.9)	5.96 (57.5)	0.272 (48.4)
Error after relocation/growing	0.360 (19.3)	0.380 (37.9)	4.62 (44.5)	0.209 (37.2)
Upstream cruise rms error	0.681 (36.6)	0.909 (90.6)	11.88 (115.)	0.541 (96.3)
Error after tendency correction	0.457 (24.7)	0.671 (66.9)	11.70 (113.)	0.994 (176.)
Error after relocation	0.171 (9.2)	0.220 (21.9)	2.94 (28.4)	0.192 (34.2)
Error after relocation/growing	0.106 (5.7)	0.104 (10.4)	1.28 (12.4)	0.064 (11.4)
Along-front cruise rms error	0.279 (15.1)	0.727 (72.5)	5.99 (57.8)	0.315 (56.0)
Error after tendency correction	0.137 (7.4)	0.325 (32.4)	3.13 (30.2)	0.189 (33.6)
Error after relocation	0.125 (6.7)	0.310 (30.9)	2.63 (25.3)	0.123 (21.9)
Error after relocation/growing	0.090 (4.9)	0.085 (8.5)	0.68 (6.6)	0.042 (7.5)

Table 1: summary of rms differences between model fields and those obtained after simulated cruise sampling followed by interpolation of synthetic observations. The standard deviations of the anomaly fields and the percentages accounted for by rms errors (in brackets) are also listed. All values correspond to 100 m depth (a level that is representative of the upper layer dynamics) and have been averaged over the horizontal domain shown in Figs. 1-12. Details on the different cruise strategies and correction methods are given in the text.

	(c_x, c_y) (km/day)	e-folding time (days)
True values	(8.0, 0.0)	4.6
Model fields	(7.7, 0.1)	4.5 – 5.4
Synoptic cruise	(7.7, 0.1)	4.4 – 5.3
Downstream cruise	(4.9, -0.2)	8.3 – 30.
Downstream cruise after relocation	(6.1, 0.3)	5.5 – 11.
Downstream cruise after relocation/growing	(6.2, 0.1)	4.5 – 6.5
Upstream cruise	(8.8, 0.2)	3.4 – 4.0
Upstream cruise after relocation	(8.2, 0.1)	4.0 – 4.2
Upstream cruise after relocation/growing	(7.6, 0.1)	4.7 – 5.6
Along-front cruise	(7.4, 0.3)	4.6 – 5.8
Along-front cruise after relocation	(8.2, 0.1)	4.1 – 4.6
Along-front cruise after relocation/growing	(8.2, 0.1)	4.3 – 4.7

Table 2: system velocity (c_x, c_y) and e-folding time (γ^{-1}) inferred from the tendency method presented in the Appendix. The method was applied to the upper layer (20–200 m); the range quoted for the growing rate corresponds to the minimum–maximum values obtained for individual levels (the system velocity did not show significant dispersion within the quoted vertical domain). True values are also listed, for an easy comparison with the results obtained for the different sampling strategies.

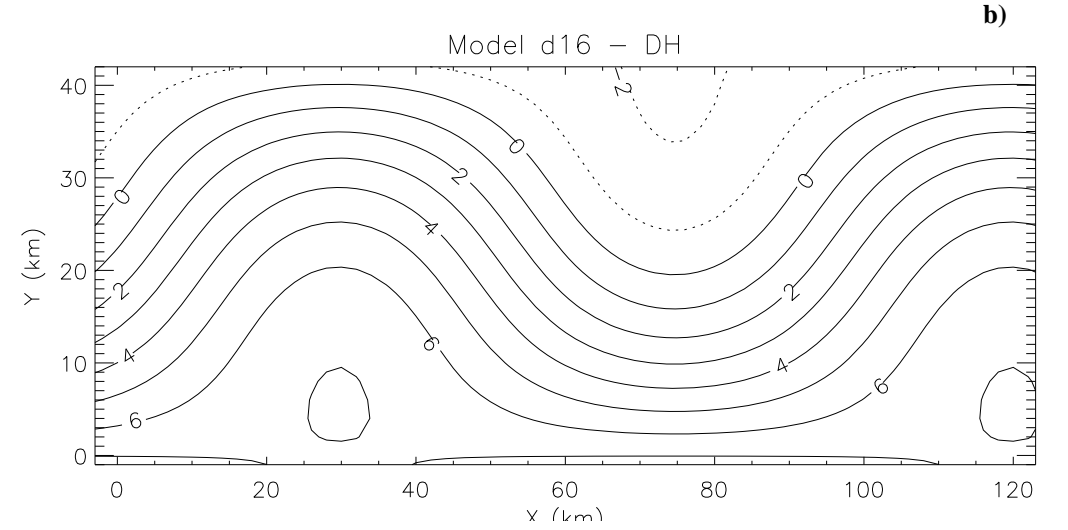
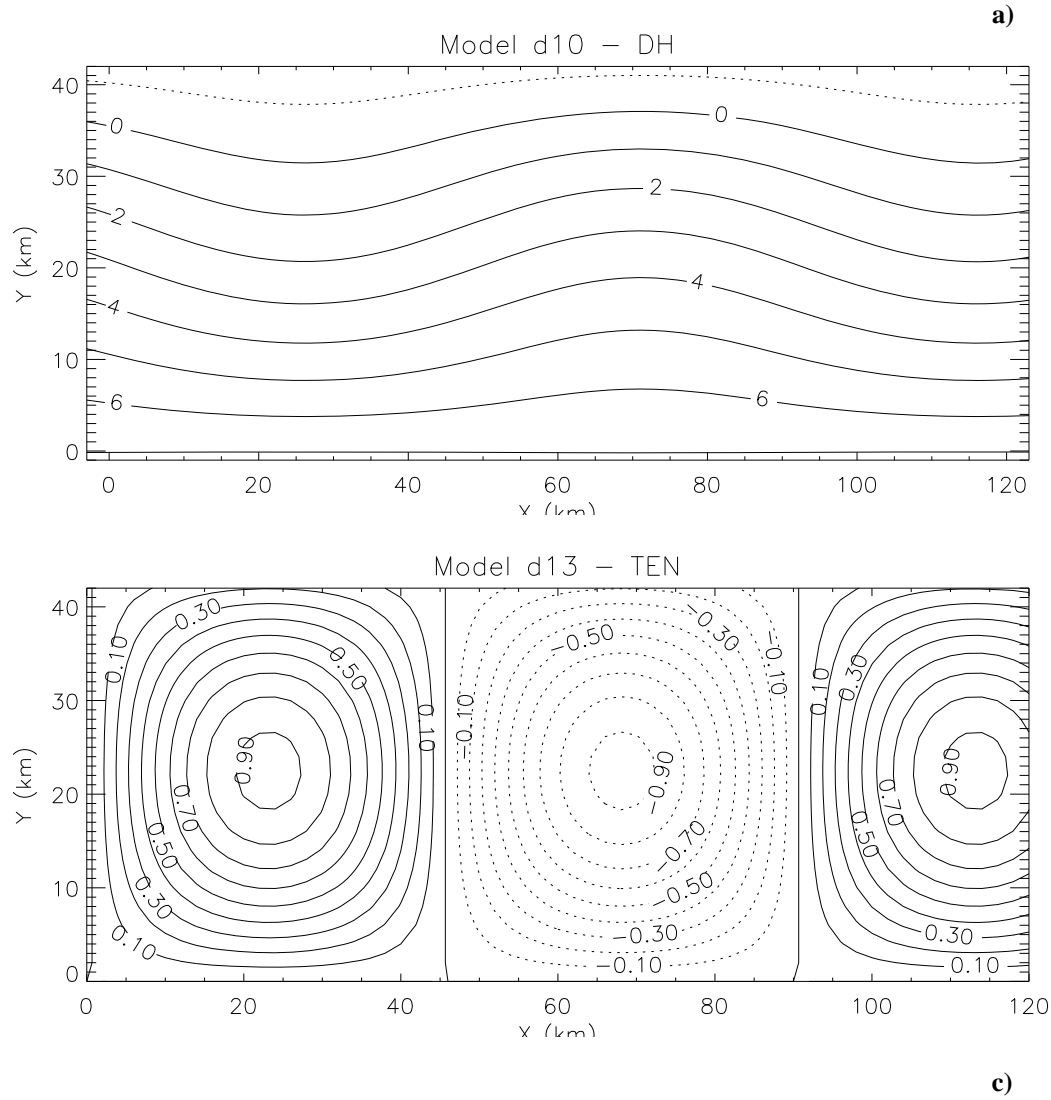


Figure 1: sequence of dynamic height fields (dyn.cm) representing a unstable baroclinic mode of 90 km wavelength embedded in a 45 km wide jet, as given by the Tang model. They correspond to days 10 (a) and day 16 (b) of the sequence (day 13 is shown in Fig. 2). (c) Dynamic height tendency (in dyn.cm/day) at day 13. All the fields of this and the following figures correspond to 100 m depth (a level that is representative of the upper layer dynamics); only the inner part of the 136x56 km² model domain is shown.

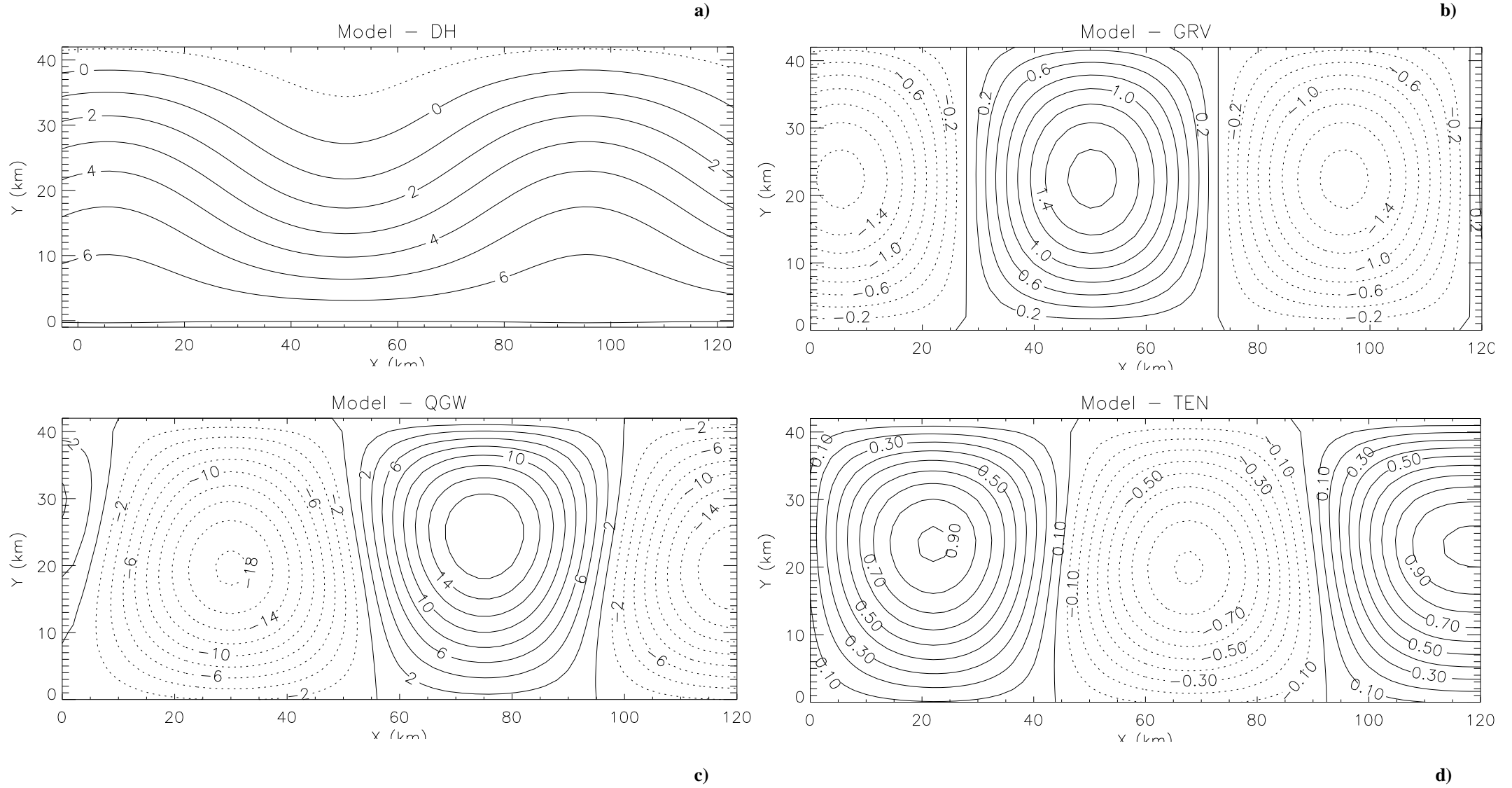


Figure 2: (a) Model dynamic height (dyn.cm) at day 13. (b) Relative vorticity (10^{-5} s^{-1}), (c) QG vertical velocity (m/day) and (d) QG tendency (dyn.cm/day) computed from the 3D model dynamic height at day 13.

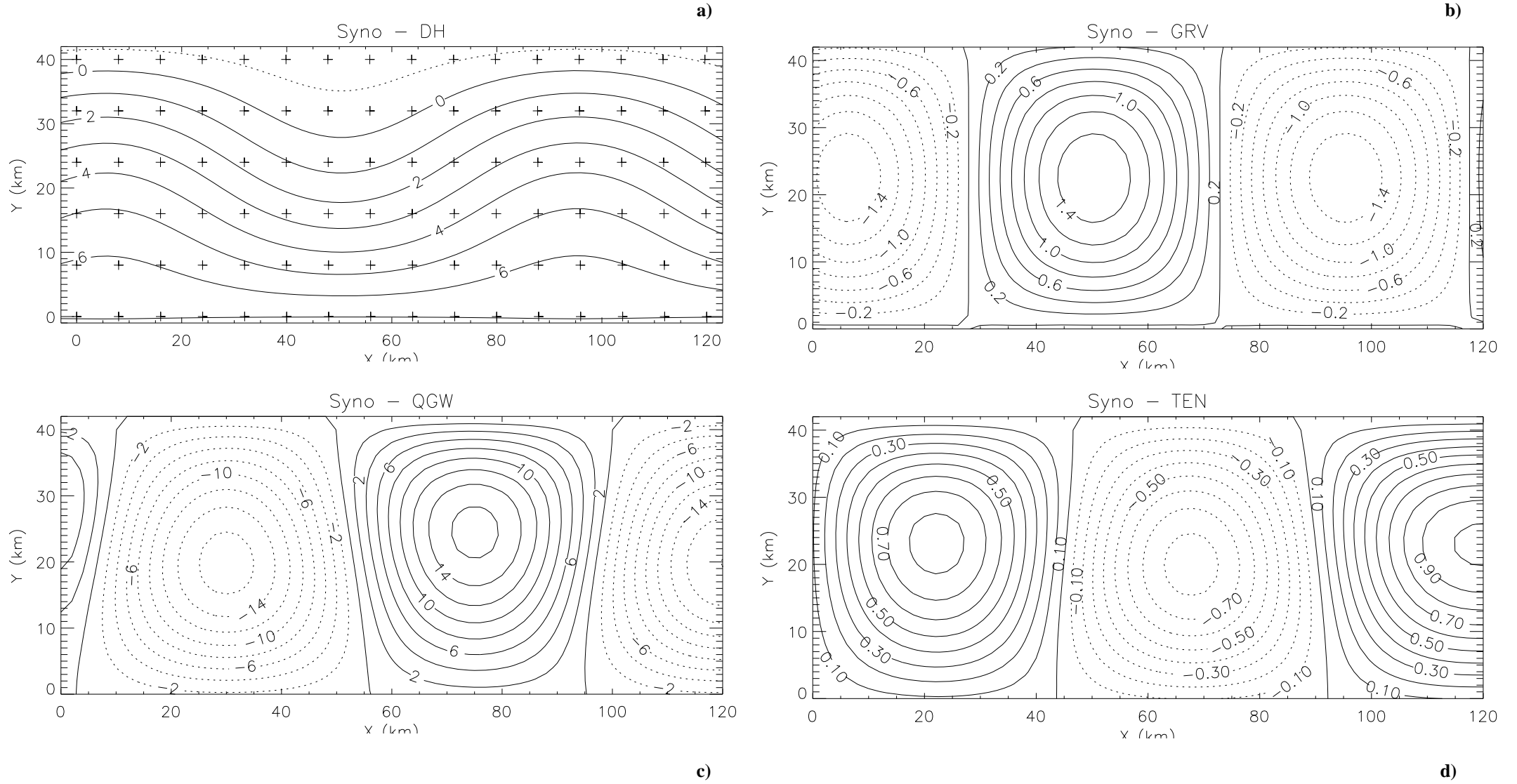


Figure 3: Results for the synoptic sampling: (a) dynamic height (dyn.cm), (b) relative vorticity (10^{-5} s^{-1}), (c) QG vertical velocity (m/day) and (d) QG tendency (dyn.cm/day). The position of 96 stations has been overlapped in (a) (other 48 stations are located beyond the boundaries of the represented inner domain).

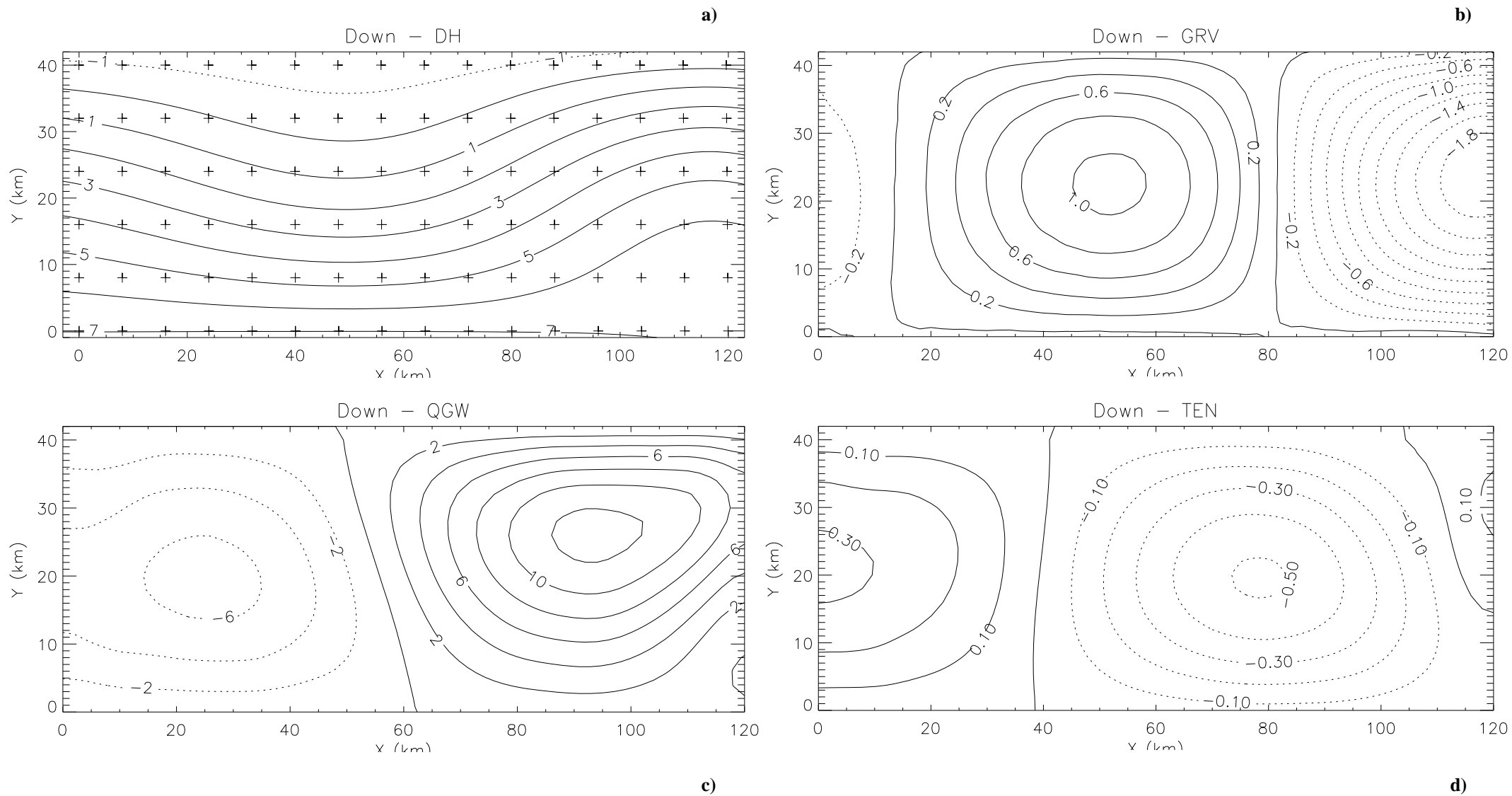


Figure 4: As in Fig. 3, but for the downstream cruise.

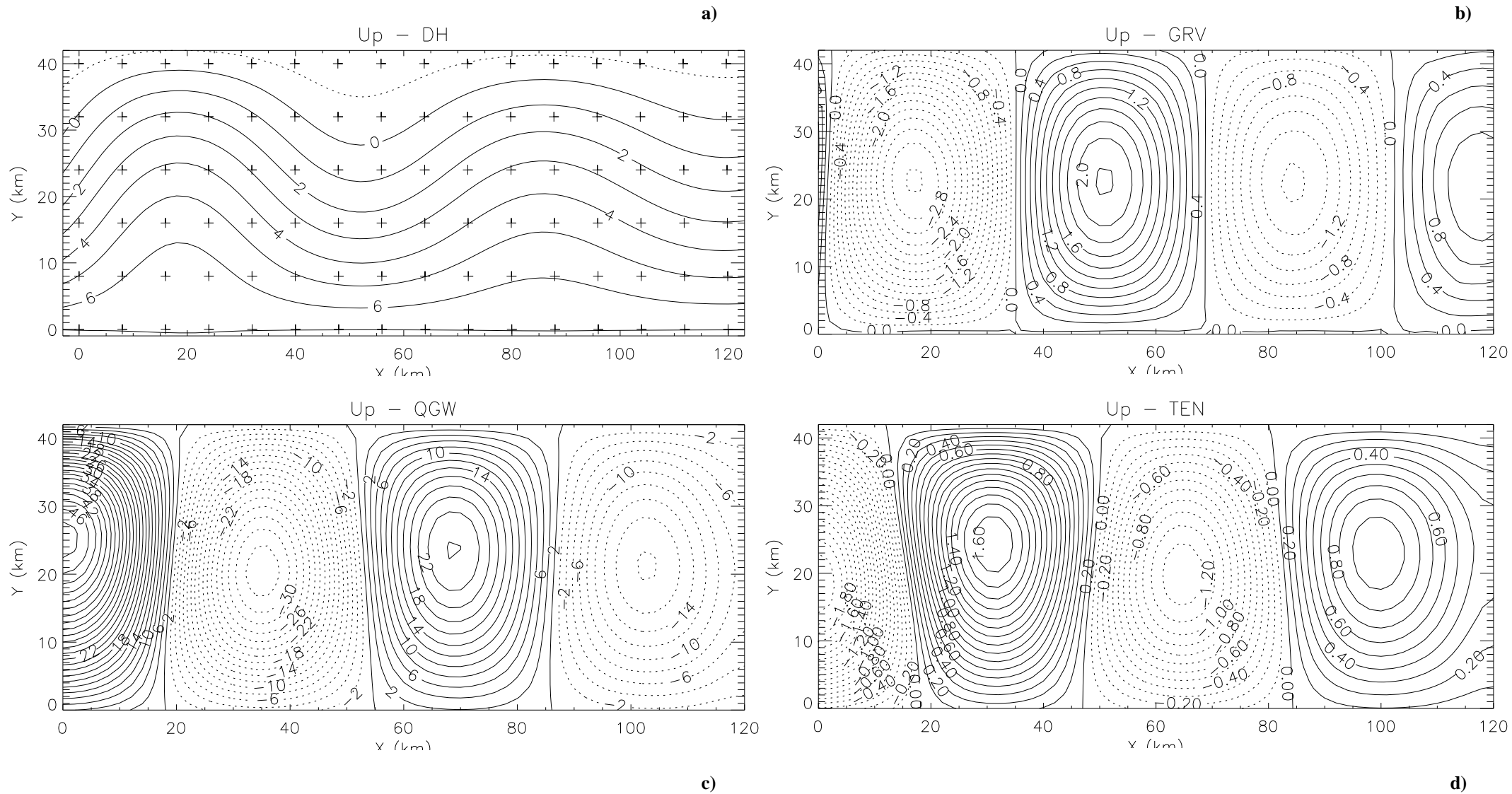


Figure 5: As in Fig. 3, but for the upstream cruise.

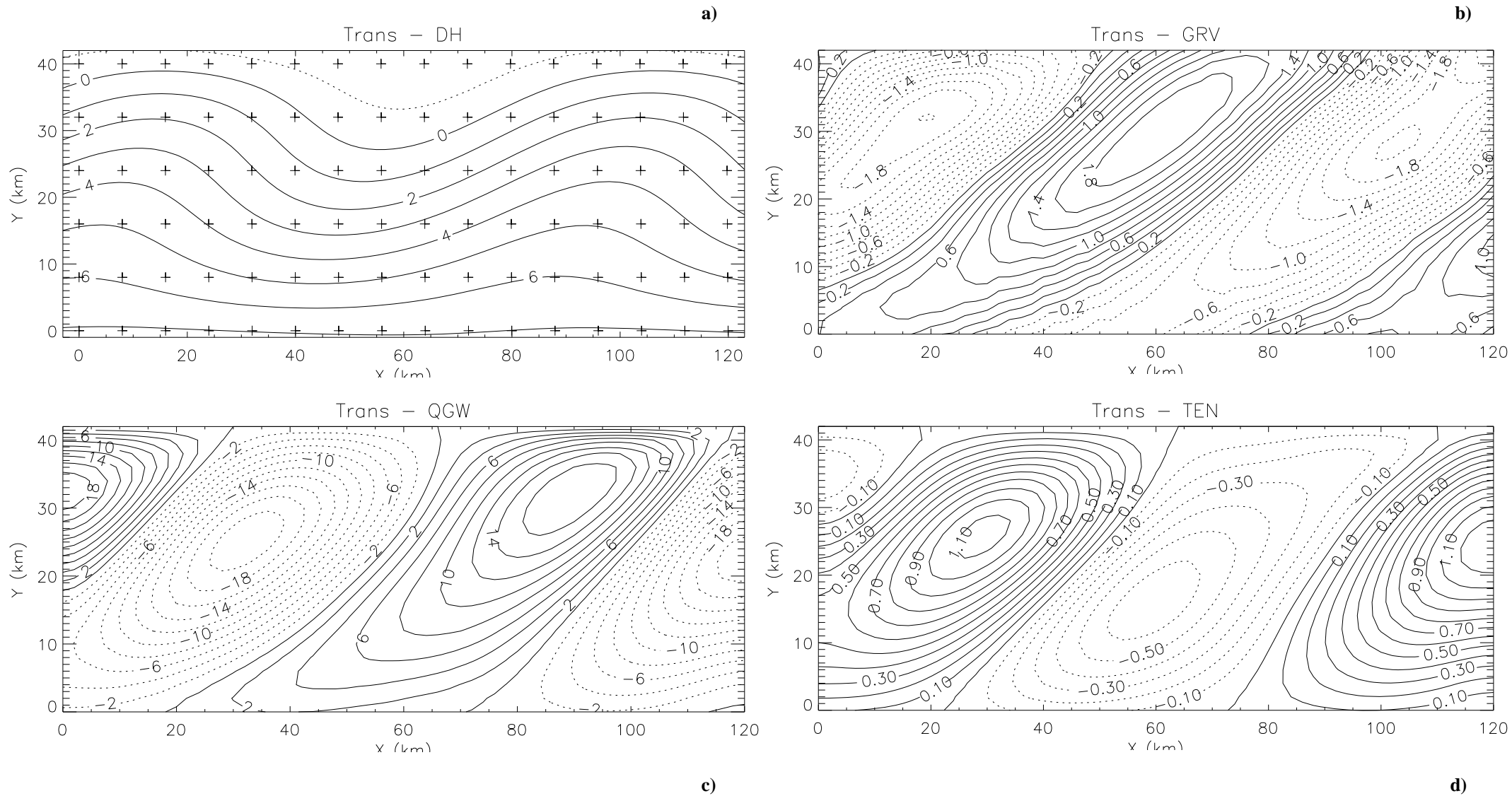


Figure 6: As in Fig. 3, but for the along-front cruise.

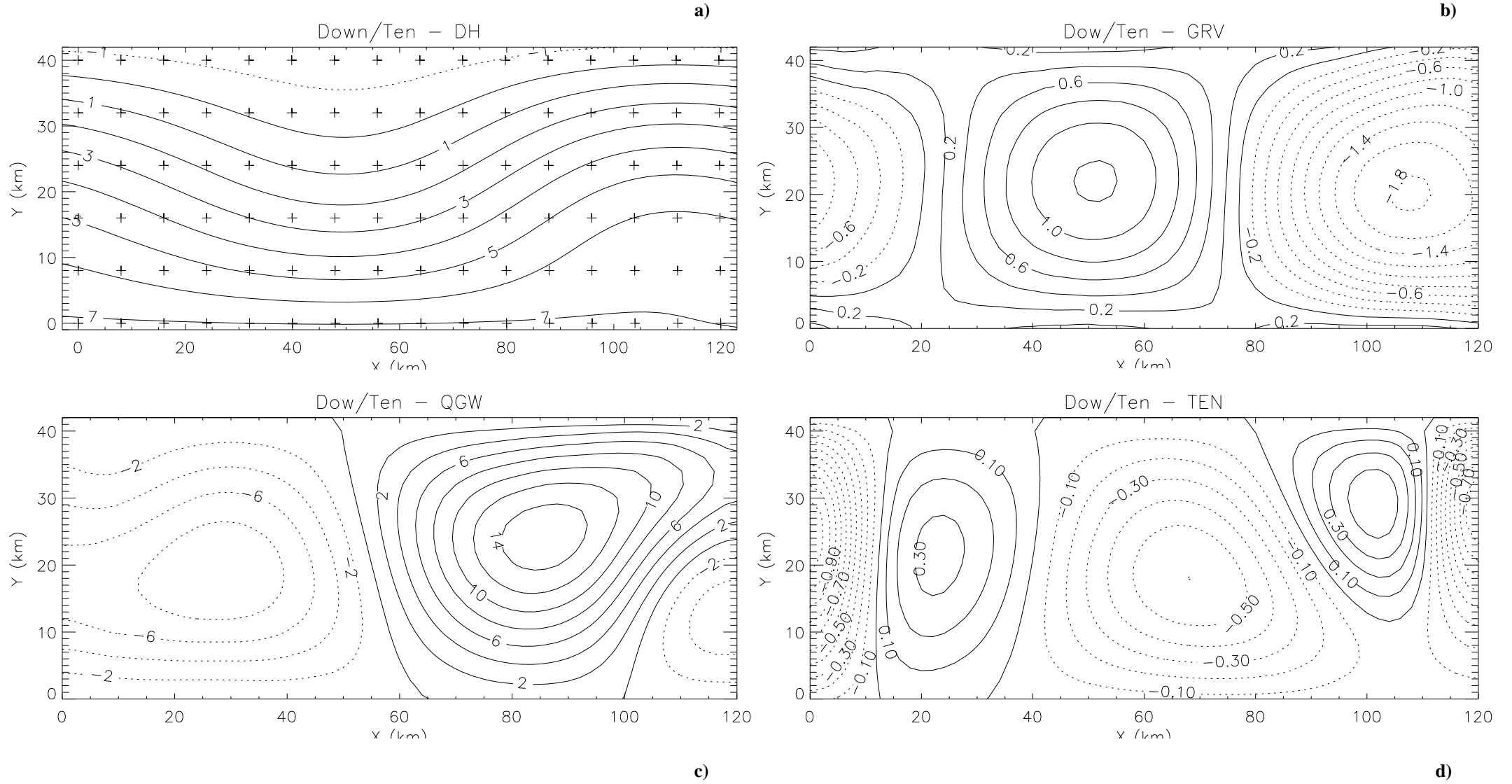


Figure 7: Results for the downstream cruise: (a) dynamic height (dyn.cm), (b) relative vorticity (10^{-5} s^{-1}), (c) QG vertical velocity (m/day) and (d) QG tendency (dyn.cm/day) obtained from the ‘pseudo-synoptic’ observations corrected following the tendency method.

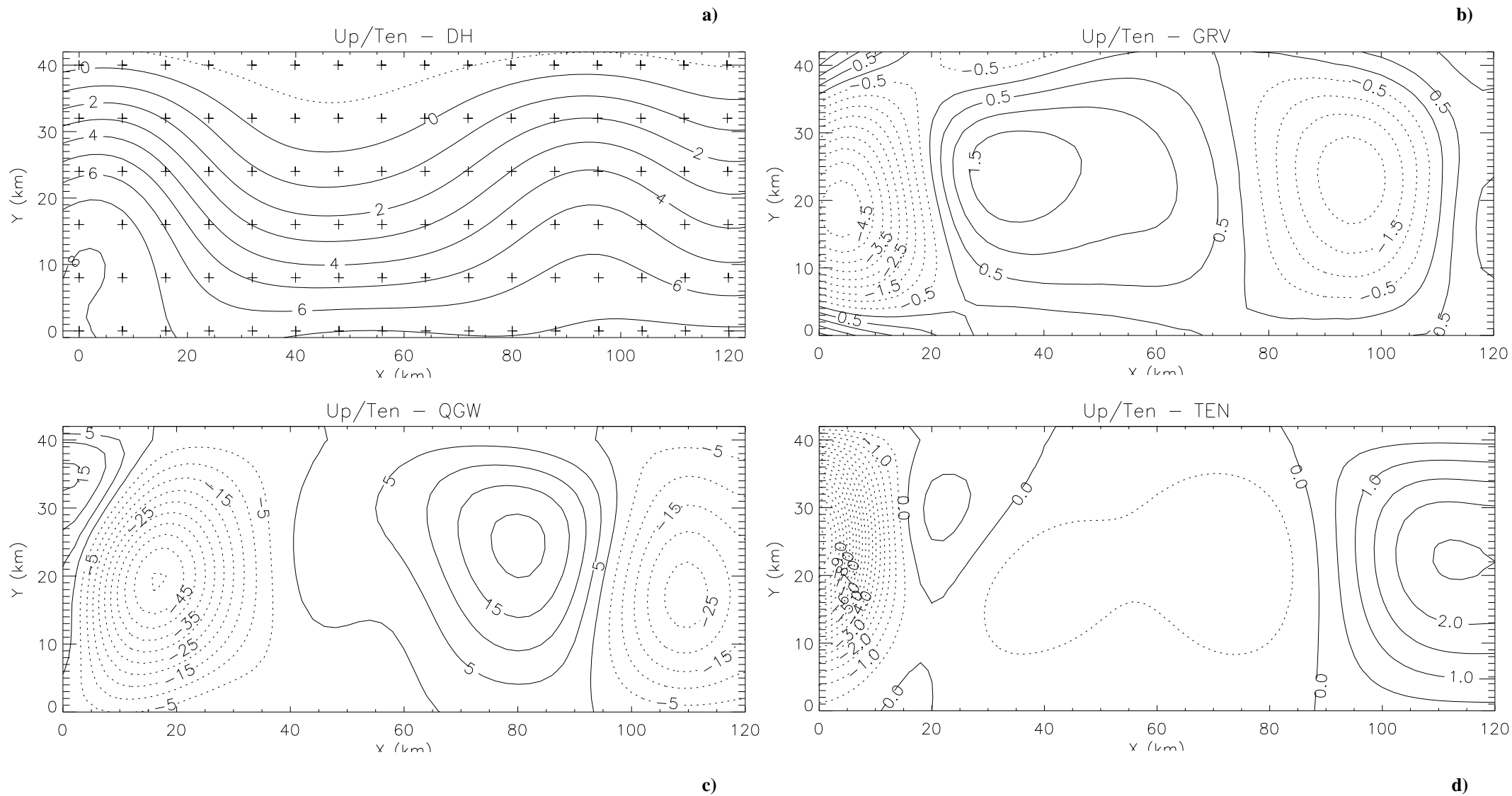


Figure 8: As in Fig. 7, but for the upstream cruise. Note that in panels b-d the spacing of isolines has changed with respect to the other figures.

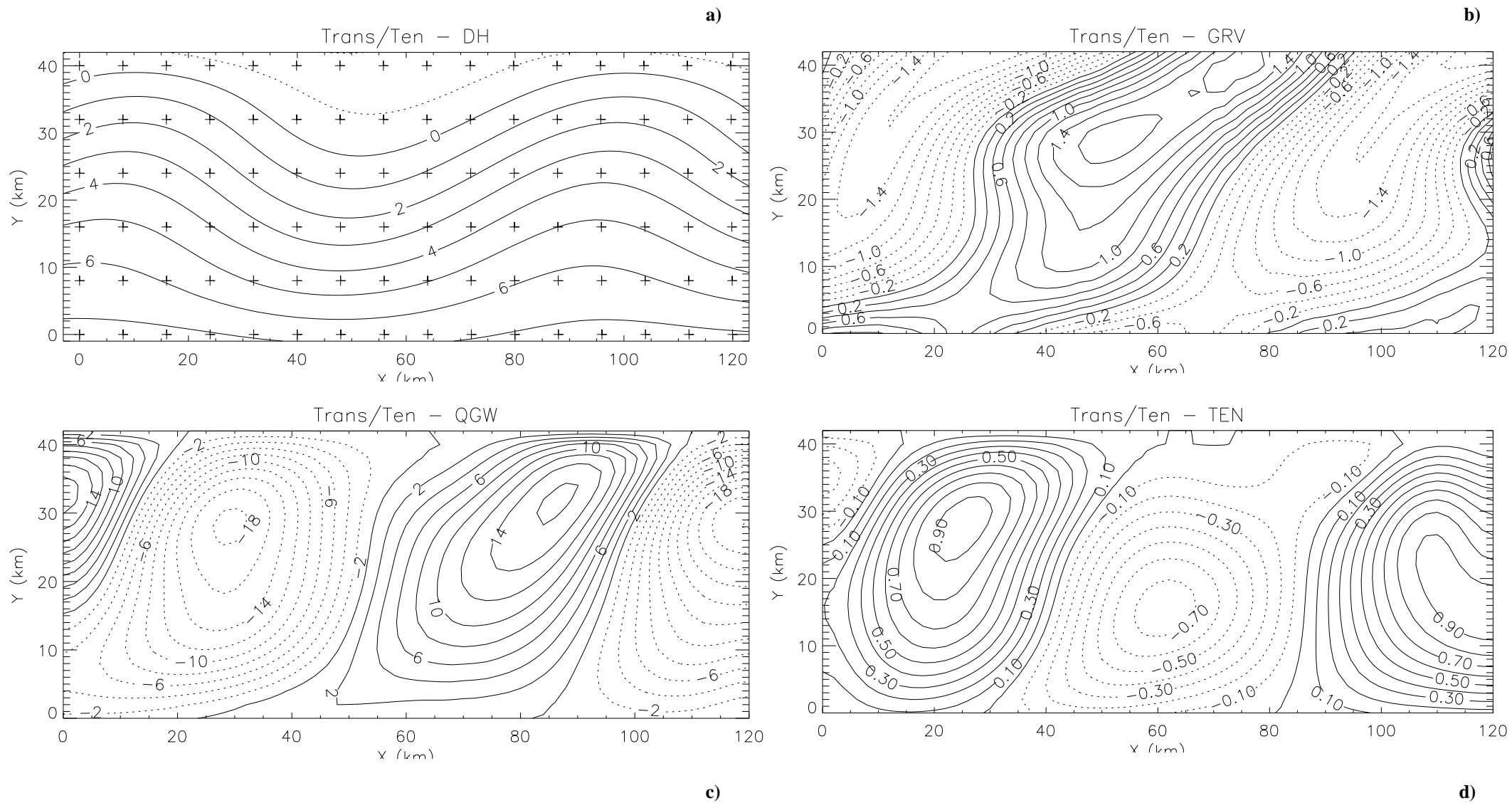


Figure 9: As in Fig. 7, but for the along-front cruise.

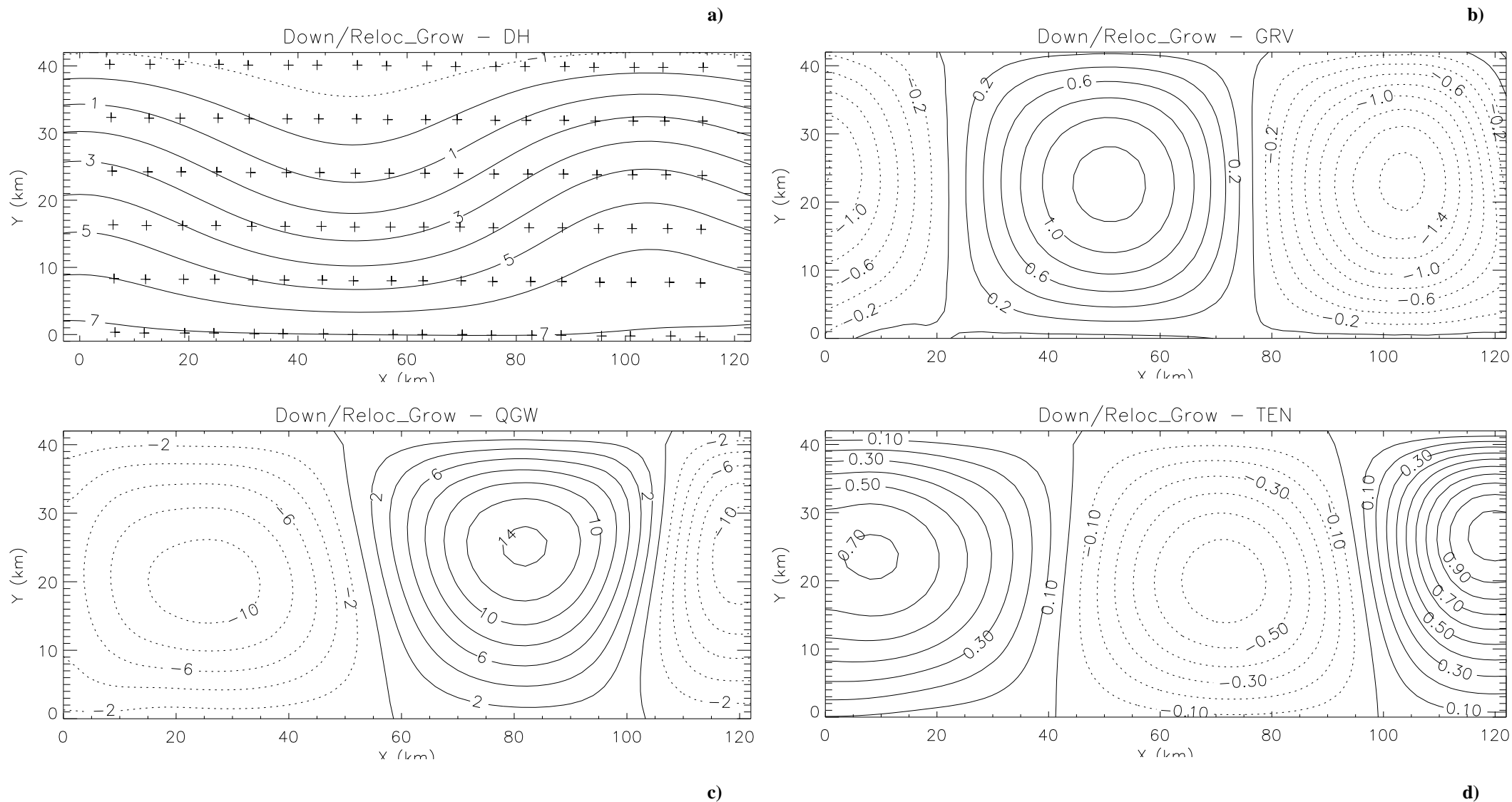


Figure 10: Results for the downstream cruise: (a) dynamic height (dyn.cm), (b) relative vorticity (10^{-5} s^{-1}), (c) QG vertical velocity (m/day) and (d) QG tendency (dyn.cm/day) obtained from the ‘pseudo-synoptic’ relocated stations with observations corrected on the basis of the estimated growing rate. The position of the relocated stations has been overlapped in (a).

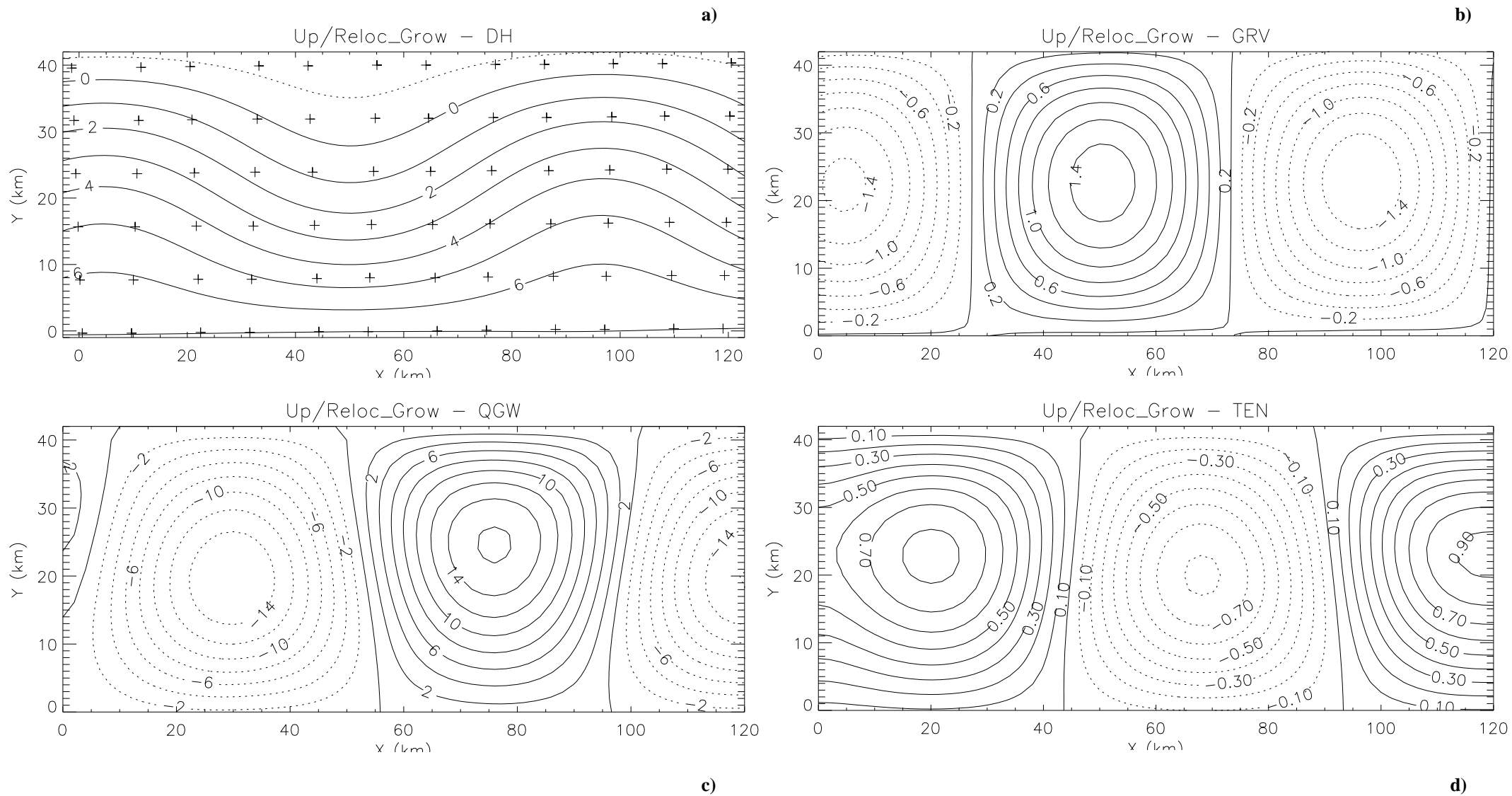


Figure 11: As in Fig. 10, but for the upstream cruise.

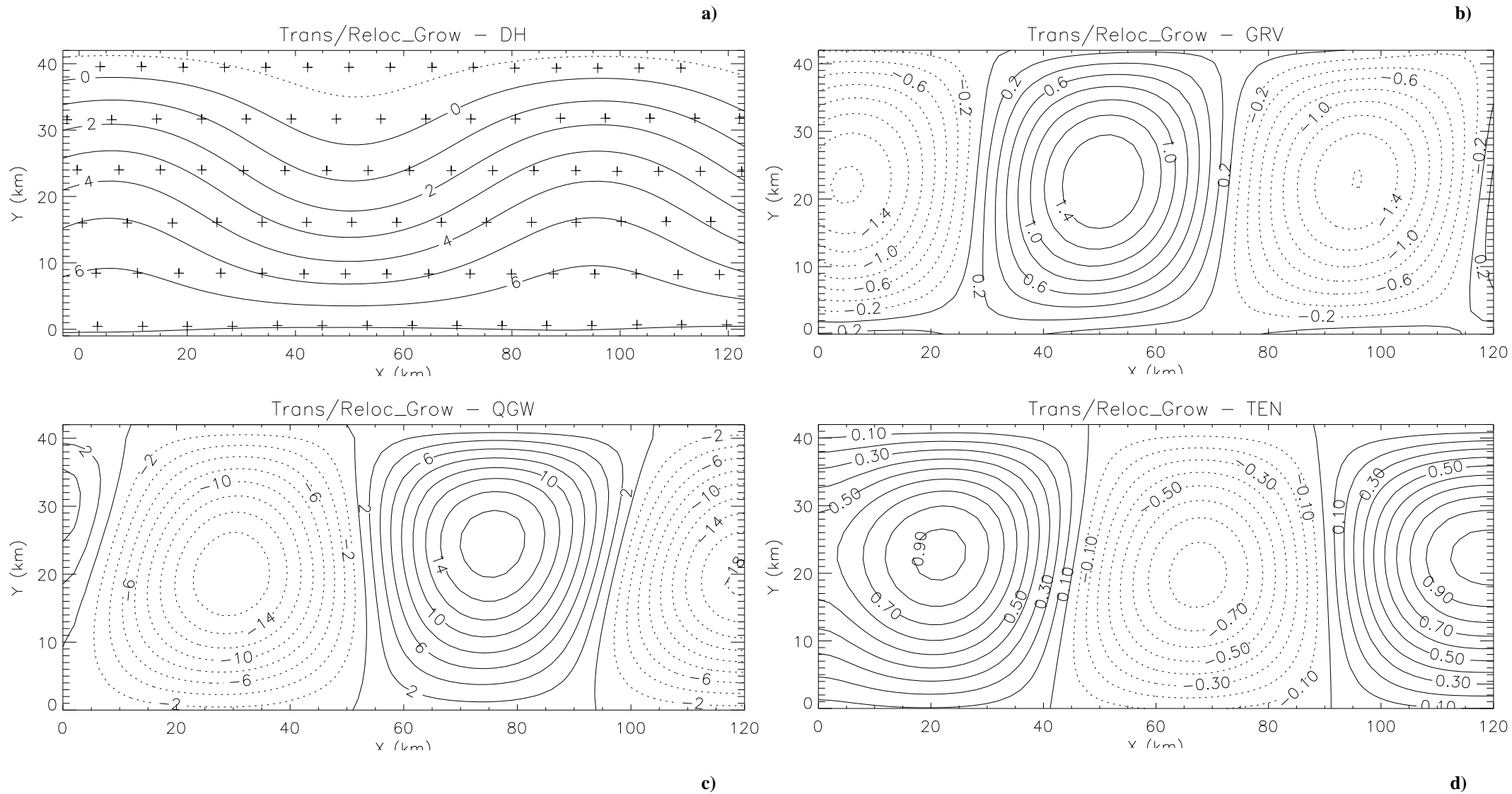


Figure 12: As in Fig. 10, but for the along-front cruise.